Lattice Boltzmann simulations for proton transport in 2-D model channels of Nafion

Yoshinobu Akinaga,†[ab] Shi-aki Hyodo[bc] and Tamio Ikeshoji[ab]

Received 26th March 2008, Accepted 11th June 2008
First published as an Advance Article on the web 29th July 2008
DOI: 10.1039/b805107k

Proton conductance in a 2-D channel with a slab-like structure was studied to verify that the lattice Boltzmann method (LBM) can be used as a simulation tool for proton conduction in a Nafion membrane, which is a mesoscopic system with a highly disordered porous structure. Diffusion resulting from a concentration gradient and migration by an electrostatic force were considered as the origins of proton transport. The electrostatic force acting on a proton was computed by solving the Poisson equation. The proton concentration in the membrane is expressed as a continuous function and the sulfonic charge is placed discretely. The space-averaged conductance of protons in a nonequilibrium stationary state was evaluated as a function of the structural parameters: namely, channel width and distribution of the sulfonic groups. The resulting space-averaged conductance deviates from the bulk values, depending particularly on the sulfonic group distribution. Details of the simulation scheme are described and the applicability of the present scheme to real membranes is discussed.

1. Introduction

Proton conductivity of a polymer electrolyte membrane (PEM) is one of the key factors that influence the efficiency of polymer electrolyte membrane fuel cells (PEFCs).[1,2] Nafion, produced by DuPont, has mainly been used as a polymer electrolyte in PEFC.[1] Nafion consists of fluorinated polyethylene (polymer backbone) and perfluorinated vinyl ether side chains with a sulfonic acid group (SO_3H) at the end of each chain. Hydrated Nafion membranes have two phases on a nanometer scale, a hydrophobic phase containing the backbone of the Nafion and a hydrophilic phase containing sulfonic acid groups and water molecules. The latter provides the means for proton conduction. High proton conductivity can only be achieved at high water contents. In this paper, we discuss a mesoscopic simulation of proton transport in a 2-D model system and its implementation. Our goal is to simulate the proton transport in PEMs with various nanostructures.

Various kinds of theoretical studies have recently been reported that simulate the proton transport in PEMs.[3–15] Paddison and coworkers[8–12] have calculated the friction coefficient of a hydronium ion moving with a constant velocity at the center of a cylindrical channel, in which SO_3^- groups represented by a point charge were distributed on the channel wall, by employing nonequilibrium statistical mechanics. They gave the proton conductance in a cylindrical channel as a correction to the zeroth-order friction coefficient obtained in bulk water. It was decomposed into three contributions arising from solvent–SO_3^-, solvent–proton, and proton–SO_3^- interactions. The computed diffusion coefficients agreed well with the measured values in experiments. The effects of dielectric saturation and ionic screening on the proton diffusion coefficients were also studied by the same group.[12] There is a cancellation of the effects due to the dielectric saturation and ionic screening. Eikerling *et al.*[13,14] estimated the proton conductivity of the Nafion membrane based on the Poisson–Boltzmann (PB) approximation and the Marcus theory. Using the slab-channel model, they computed both the proton density distribution and the electrostatic potential in the channel by solving the PB equation.[13] Their results indicate that the local proton mobility in the first water monolayer near the channel wall is considerably lower than that in the bulk region. Based on those results, Eikerling *et al.*[14] computed the proton conductivity of a cylindrical channel with a fixed number of SO_3^- groups with various channel radii using a two-state model for the proton transport mechanism, and eventually estimated the specific membrane conductivity, which agreed well with typical experimental data. Both studies by Paddison *et al.* and Eikerling *et al.* have shown that resistance to the proton motion because of SO_3^- groups plays an important role in the membrane conductivity.

The model proposed by Paddison *et al.* can be used to estimate the proton mobility in a nonequilibrium stationary state. Moreover, the relative importance of various contributions from different physical origins can be analyzed. In their model, however, the hydronium ion moves only in the center of the channel. Therefore, the density variation of the proton in the channel is not explicitly included, although the model was extended later so that the effect of the ionic screening and dielectric saturation can be taken into account. In the work by

[a] *Research Institute for Computational Sciences (RICS), National Institute of Advanced Industrial Science and Technology (AIST), Umezono 1-1-1, Tsukuba, Ibaraki 305-8568, Japan. E-mail: akinaga@info.human.nagoya-u.ac.jp*
[b] *CREST, Japan Science and Technology Corporation (JST), Honcho 4-1-8, Kawaguchi, Saitama 332-0012, Japan*
[c] *TOYOTA Central R&D Labs., Inc., Nagakute, Aichi 480-1192, Japan*
† Present address: Graduate School of Information Science, Nagoya University, Furo-cho, Nagoya 464-8601, Japan.

Eikerling *et al.*, the density distribution of the proton was taken into account at the PB level of approximation. The PB equation was, however, solved only for the equilibrium state.

The lattice Boltzmann method (LBM) has been used in recent years to solve mesoscopic problems.[16,17] Its simple algorithm makes the LBM a powerful tool for simulating complex fluids and flows in highly disordered nanoscale porous structures. Because of its ability to adopt complex structures, the LBM is regarded as a very appropriate method for simulating proton transport in PEMs, such as Nafion. To apply the LBM to solve proton transport problems, the diffusion equation has to be solved instead of the ordinary Navier–Stokes equations. Several authors have shown that the LBM can deal with both the diffusion equation and the Navier–Stokes equation.[16,18] The LBM has also been shown[19–21] to be able to handle electrochemical systems involving inhomogeneous reactions such as those in batteries. In the work by He and Li,[21] an LBM scheme for electrochemical systems has been proposed where several transport processes, namely, convection, diffusion, migration by an electrostatic force, and electrode reactions are involved.

In the present study, diffusion resulting from a concentration gradient and migration by an electrostatic force that is computed by solving the Poisson equation are considered. The proton is treated as residing in a continuum medium distributed in the water region. The strategy to obtain the average mobility is as follows: (1) we define the structures of the model channel and (2) the continuum proton distribution in the channel is obtained according to the PB theory. (3) A uniform electric field is applied to invoke a current. (4) By measuring the magnitude of the current at each point, the average mobility of the proton is computed. Such an approach includes both factors mentioned before: the nonequilibrium stationary state and the proton distribution in the channel.

Because the membrane consists of channels with various sizes and with various distributions of SO_3^-, it is important to evaluate the transport properties of each channel to estimate the proton conductivity of the whole membrane. For this reason, we focused on the basic transport property of a proton in a two-dimensional single channel with a slab-like structure, eliminating the factor of random structure. Two structure parameters of the model channel were examined; the channel width R and the separation d between SO_3^- groups. The variation of R can be regarded as variation of the water content of the membrane, *i.e.* the number of water molecules per SO_3^- group. The variation of d corresponds to the variation of the equivalent weight, *i.e.* mass of the membrane per SO_3^- group. Because the present scheme can be easily extended to the 3-D case due to the simplicity of programming the LBM, a quantitative estimation of the membrane conductance in practical use will be possible using 3-D porous structures.

It is obvious that a "point charge" in a 2-D space is equivalent to a line charge with infinite length in a 3-D space. Because the electrostatic field created by a line charge has a different dependency on the radial distance r compared to the electrostatic field of a point charge (r^{-1} and r^{-2} for a line charge and a point charge, respectively), 2-D models in this work give only a qualitative result of how the proton conductivity behaves as a function of the parameters R and d, which reflect the macroscopic membrane structure parameters such as water content and equivalent weight. Based on the results of the present study, we can verify our methodology as a tool for simulating proton conduction in a membrane, and use it for a quantitative study of 3-D porous membrane systems. From such a viewpoint, the exact functional form of the attractive potential created by each SO_3^- group is not essential in this paper; rather, the configuration of each potential source should be a critical factor. For such reasons, the 2-D description is sufficient for the present purpose. We also point out that using 2-D models saves a considerable amount of computational time. Therefore, we concluded that a 2-D description is suited for the present purpose.

In macroscopic systems, the interaction between a fluid and the solid surface can be well described by the stick condition, in which the flux parallel to the interface is set to zero at the boundary. On the other hand, when the slip velocity cannot be ignored, as in the case of microscopic flows, the slip condition is more appropriate. Most LBM simulations have so far employed the stick condition because of its physical validity and computational convenience. In diffusion problems, however, a necessary and sufficient boundary condition in nonreacting diffusion problems is that the flux across the fluid–solid interface vanishes and there is no physical basis to set the flux parallel to the interface to zero. Although the stick condition is desirable for computational convenience, ignoring the flux parallel to the interface might lead to an artificial error in estimating the conductivity. Thus, we used the slip conditions at the fluid–solid interface after examining the effect of using the stick condition in electrochemical diffusion systems.

The paper is organized as follows. Section 2 describes the 2-D model adopted in the present work and the fundamental formulae of the diffusion LBM in the ionic system. Numerical results and discussions will be given in section 3. Finally, section 4 concludes the study.

2. Theory

We describe the 2-D model used in the present study. The necessary formalism of the LBM for use in this work, as well as details of the boundary conditions, are also described.

2.1 2-D slab channel

Various models have been proposed for mimicking the water region in Nafion, namely; cluster–network, modified core–shell, local-order, lamellar, sandwich-like, and rod-like models.[1] In the present work, we adopted the sandwich-like model as described in the Introduction.

Fig. 1a illustrates a 2-D model of a pore in a Nafion membrane. The aqueous region, which consists of protons and solvent water, is sandwiched by the polymer backbone regions. Wall charges that mimic the fixed SO_3^- groups, indicated by full black circles, are distributed at the interface between the aqueous region and the polymer region. Each wall charge is covered by a hydration shell as represented in dark gray in Fig. 1a. The proton was allowed to move in the aqueous region under the influence of the electrostatic potential from the SO_3^- groups, but not allowed to enter the hydration shells. The hydration shells prevent the proton from binding to SO_3^- groups. The width of the hydration shells was set to 3 Å, which is close to the size of a solvent water molecule.

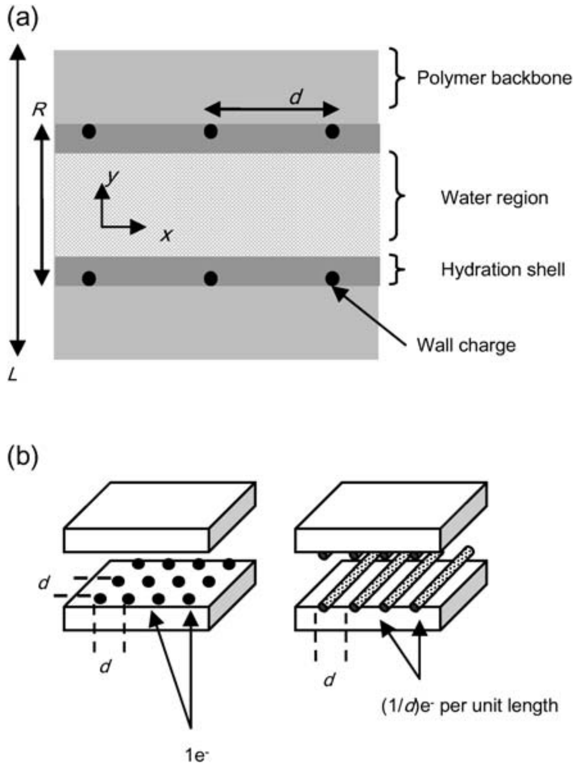

Fig. 1 The 2-D sandwich model of ion channels in Nafion. (a) The model channel used in the present calculation. Light gray, polymer region (P); dark gray, hydration shell (HS); hatched, water region (W); full circle, point charges representing SO_3^- groups. The point charges were placed between the W–HS and HS–P interfaces, separated by 1 Å from the HS–P interface and 3 Å from the W–HS interface. (b) The way to project a 3-D sandwich model (left) to a 2-D model (right).

The relative dielectric constant ε_r in Nafion may have different values depending on the position in a membrane. Because a typical value of ε_r for resins such as Teflon and paraffin lies within the range of 2.0–2.5, $\varepsilon_r = 2.0$ was assumed for the polymer region. Hereafter, "water region" means the region in which the proton can move around, *i.e.* the aqueous region except for hydration shells, and will be denoted by "W". "HS" and "P" will be used to refer to the hydration shell and the polymer backbone region, respectively. According to dielectric response measurements, the dielectric function of the Nafion membrane varies depending strongly on the water content.[22–24] The assumption of constant ε_r (for example, the bulk value) for the whole region cannot describe properly the dielectric property of water in the Nafion membrane of various water contents. Paddison *et al.* estimated the dielectric constant as a function of the radial position within a cylindrical channel based on a statistical mechanical point of view.[25–27] According to their estimation the value of ε_r around the channel center is close to the value of the bulk water. It decreases continuously and reaches nearly 10 (ref. 25) and 2 (ref. 26 and 27) in the proximity of the SO_3^- group due to the interaction between the dipole moment of water molecules and the negative charge of SO_3^- groups. The region where the water molecules can be regarded as "free water" is rather restricted, especially for the low water content, $\lambda = 6$; λ is defined as a ratio of the number of water molecules against the number of SO_3^- groups. These results indicate that while the bulk value of ε_r well describes the water around the channel center, the value of ε_r in the proximity of SO_3^- groups should be different. Thus, in the W region, we used $\varepsilon_r = 78$. For the HS region, ε_r may be less than 10 because of the strong dielectric saturation.[25–27] The possible lowest limit in this region can be estimated based on the electronic polarizability of a water molecule, 1.45 (ref. 28) and the high frequency limit of the water dielectric function, 4.5–6.0 (ref. 29). These values imply that the rotation of the water molecules is inhibited around the SO_3^- group. However, a recent first-principle molecular dynamics simulation of the proton in Nafion suggests that the motion of the water molecules hydrating the SO_3^- groups is not strongly restricted.[30] Therefore, we varied ε_r of HS over a wide range of 2.0–78.0 to find its influence on the average proton mobility.

SO_3^- charges are represented by line charges with an infinite length in the perpendicular direction to the 2-D plane. The amount of charge σ per unit length was determined so that the density of the negative charge per unit area of the polymer–water interface corresponds to that of the regularly arranged point charges with a lattice distance d (see Fig. 1(b)). When the separation of adjacent wall charges is 10 Å, for example, σ is $-0.1e$ Å^{-1}.

Haubold *et al.* estimated the thickness of the polymer backbone, including side chains and ionic groups, to be approximately 30–35 Å.[31] According to Dreyfus *et al.*, the shortest distance between micelles in the Nafion117 membrane varies from 24.11 to 34.44 Å.[32] The influence was confirmed to be small by calculating the proton conductivity by varying the thickness of the polymer region from 10 to 50 Å. Thus, we will present the results obtained only for the thickness of the polymer regions equal to 30 Å.

2.2 Lattice Boltzmann equations for electromigration–diffusion systems

The time-evolution equation for the single-component LBM can be generally written as[16,17]

$$g_\alpha(\boldsymbol{r} + \boldsymbol{c}_\alpha \Delta t) = (1 - \omega) g_\alpha(\boldsymbol{r}) + \omega\, g_\alpha^{\mathrm{eq}}(\boldsymbol{r}) \tag{1}$$

where Δt is the time step, $\boldsymbol{c}_\alpha$ ($\alpha = 1$ to b, where b is determined by the type of the lattice employed) is a discrete velocity, g_α is the density distribution function of the fluid species (*i.e.*, proton) corresponding to the velocity $\boldsymbol{c}_\alpha$, g_α^{eq} is the equilibrium distribution function of the fluid species corresponding to the velocity $\boldsymbol{c}_\alpha$, and ω is the frequency for Bhatnagar–Gross–Krook (BGK) collision. We employed a 2-D, nine velocity lattice (2D9V) in the present work. The set of $\boldsymbol{c}_\alpha$ in the 2D9V lattice is expressed as

$$\boldsymbol{c}_\alpha = \begin{cases} 0 & \alpha = 0 \\ \left(\cos\left[\frac{\alpha-1}{2}\pi\right],\ \sin\left[\frac{\alpha-1}{2}\pi\right]\right) & \alpha = 1,2,3,4 \\ \sqrt{2}\left(\cos\left[\frac{\alpha-5}{2}\pi + \frac{\pi}{4}\right],\ \sin\left[\frac{\alpha-5}{2}\pi + \frac{\pi}{4}\right]\right) & \alpha = 5,6,7,8 \end{cases} \tag{2}$$

The equilibrium function can be written as

$$g_\alpha^{\mathrm{eq}} = W_\alpha \rho \left[1 + \frac{m\boldsymbol{c}_\alpha \cdot \boldsymbol{u}}{kT} + \frac{m^2(\boldsymbol{c}_\alpha \cdot \boldsymbol{u})^2}{2(kT)^2} - \frac{mu^2}{2kT}\right], \tag{3}$$

where k, m, ρ, and T are the Boltzmann constant, the mass of the fluid particle which is regarded as a hydronium ion in this study, density of the fluid species, and the temperature, respectively. $\boldsymbol{u}$ is the convection velocity of the solvent, while we assumed $\boldsymbol{u} = 0$ in this work. The weight factors $\{W_\alpha\}$ have values of 4/9 for $\alpha = 0$, 1/9 for $\alpha = 1$ to 4, and 1/36 for $\alpha = 5$ to 8. The fluid density, ρ, at each lattice point $\boldsymbol{r}$ is obtained by summing up all components of g_α:

$$\rho(\boldsymbol{r}) = \sum_{\alpha=0}^{8} g_\alpha(\boldsymbol{r}). \tag{4}$$

The collision frequency ω is related to the relaxation time τ by

$$\omega = \left(\frac{\tau}{\Delta t} + \frac{1}{2}\right)^{-1}. \tag{5}$$

In diffusion problems, the BGK relaxation time τ is related to the diffusion coefficient D, which is equivalent to the mobility *via* the Nernst–Einstein relation, as[16]

$$\tau = \frac{mD}{kT}. \tag{6}$$

D was assumed to be constant in the W region, *i.e.*, τ is independent of position. In ionic systems, the electrostatic force plays a critical role in transport phenomena. By incorporating the electrostatic force, one obtains the time-evolution equation of the distribution functions $\{g_\alpha\}$ for the diffusion–electromigration problem as

$$g_\alpha(\boldsymbol{r} + \boldsymbol{c}_\alpha \Delta t) = (1-\omega) g_\alpha(\boldsymbol{r}) + \omega g_\alpha^{\mathrm{eq}}(\boldsymbol{r}) + \left(1 - \frac{\omega}{2}\right) \frac{ze(\boldsymbol{c}_\alpha - \boldsymbol{u}) \cdot \nabla\phi}{kT} g_\alpha^{\mathrm{eq}}, \tag{7}$$

where ϕ is the electrostatic potential and ze is the charge on the fluid ion. One can prove, using the Chapman–Enskog expansion, that eqn (7) becomes the following electromigration–convection–diffusion equation for the proton density ρ.

$$\frac{\partial\rho}{\partial t} + (\boldsymbol{u} \cdot \nabla)\rho = \nabla \cdot (D\nabla\rho) + \nabla \cdot \left(\frac{zDe\rho}{kT} \nabla\phi\right) \tag{8}$$

The electrostatic field $\nabla\phi$ is the sum of the electrostatic field $\nabla\phi_0$ created by the charge density determined by SO_3^- charges plus proton density and a uniform electric field $\boldsymbol{E}$ applied along the x-direction in Fig. 1a. The lattice separation was taken to be 1 Å.

2.3 Lattice Boltzmann equations for the Poisson equation

The electrostatic potential ϕ_0 created by the charge density is obtained as the solution of the Poisson equation

$$\nabla^2 \phi_0 = \frac{q}{\varepsilon_0 \varepsilon_r}. \tag{9}$$

In the above expression, ε_0 and ε_r mean the dielectric constant of the vacuum and the relative dielectric constant of the medium that is under consideration, respectively. In our work, the medium is either the aqueous solution (water) or the polymer backbone of Nafion. q is the charge density distribution that is given as the sum of the proton distribution, ρ, and the SO_3^- charge of the Nafion. Eqn (9) may be solved by various numerical methods such as successive over-relaxation and multigrid techniques.[33,34] In the present work, we solved eqn (9) by the LBM as well, in accordance with the approach by He and Li.[21]

Introducing a set of distribution functions $\{h_\alpha\}$, which is related to the electrostatic potential ϕ_0 by

$$\phi_0(\boldsymbol{r}) = \sum_{\alpha=0}^{8} h_\alpha(\boldsymbol{r}), \tag{10}$$

one can obtain the solution of eqn (9) by solving the following lattice Boltzmann equation for $\{h_\alpha\}$

$$h_\alpha(\boldsymbol{r} + \boldsymbol{c}_\alpha \Delta t) = (1 - \omega_\phi) h_\alpha(\boldsymbol{r}) + \omega_\phi h_\alpha^{\mathrm{eq}}(\boldsymbol{r}) + W_\alpha \frac{q(\boldsymbol{r})}{\varepsilon_0 \varepsilon_r}, \tag{11}$$

where

$$h_\alpha^{\mathrm{eq}}(\boldsymbol{r}) = W_\alpha \phi_0(\boldsymbol{r}), \tag{12}$$

at the stationary state. The 2D9V lattice was used in solving the Poisson equation by the LBM.

2.4 Boundary conditions

Periodic boundary conditions were applied to both the x- and y-directions. After solving eqn (9), a uniform electric field parallel to the channel wall (x-axis; see Fig. 1) was added to $\nabla\phi_0$ to induce a proton flow. At the channel walls, both ϕ_0 and ρ need to satisfy suitable boundary conditions.

Boundary condition for the electrostatic potential. To calculate the electrostatic potential, we need to take account of the dielectric interfaces between the W, HS, and P regions. Because the dielectric constant in the polymer is much smaller than that in water, it is expected that the effect of image charges has a non-negligible effect on the electrostatic force acting on the proton. According to classical electromagnetics,[35] the gradient of an electrostatic potential has a discontinuity at a dielectric interface while the potential itself is continuous. If we, for simplicity, ignore HS and consider the interface between the W and P regions, the boundary condition at the W–P dielectric interface can be expressed as follows:

$$\begin{aligned} \phi_W|_s &= \phi_P|_s \equiv \phi_s \\ \varepsilon_W \boldsymbol{n}_W \cdot \nabla\phi_W|_s &+ \varepsilon_P \boldsymbol{n}_P \cdot \nabla\phi_P|_s = 0, \end{aligned} \tag{13}$$

where ε_W and ε_P are the relative dielectric constant in the water and polymer regions, respectively, and the index $|_s$ means that the value is evaluated at the interface. $\boldsymbol{n}_W$ and $\boldsymbol{n}_P$ are unit vectors normal to the W–P interface, as shown in Fig. 2. In the above expression, we introduced the potential functions ϕ_W and ϕ_P so that the electrostatic potential ϕ in the whole system is expressed as

$$\phi(\boldsymbol{r}) = \begin{cases} \phi_W(\boldsymbol{r}) & \boldsymbol{r} \in \text{ water region} \\ \phi_P(\boldsymbol{r}) & \boldsymbol{r} \in \text{ polymer region} \end{cases}. \tag{14}$$

ϕ_s is the value of the potential shared by ϕ_W and ϕ_P at the interface. We introduce the above conditions into an LBM framework in a way similar to the work of He and Li.[21] When the dielectric interface is placed horizontally between the water

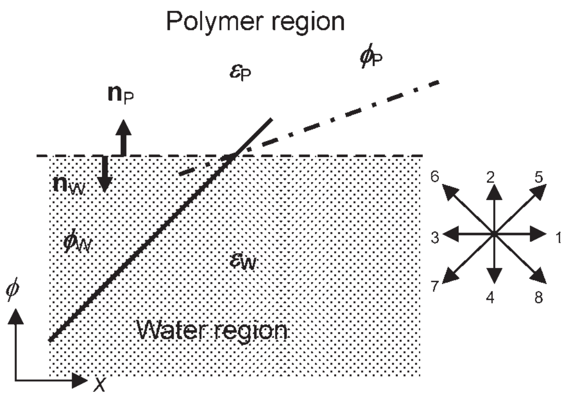

Fig. 2 A schematic view of the boundary condition for the electrostatic potential ϕ at a dielectric interface. Thin line, electrostatic potential in the water region (ϕ_W); broken line, electrostatic potential in the polymer region (ϕ_P); dotted line, dielectric interface. $\boldsymbol{n}_P$ and $\boldsymbol{n}_W$ are unit vectors normal to the interface. Discrete velocity components of the 2D9V lattice are shown for convenience.

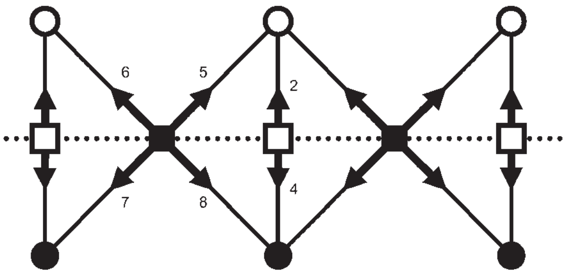

Fig. 3 Sub-lattice points at a fluid–solid boundary. Open circles, lattice points in the fluid region; full circles, lattice points in the solid region; open squares, sub-lattice points that intersect one fluid–solid link; full squares, sub-lattice points shared by two fluid–solid links; dotted line, the interface.

region on the lower side and the polymer region on the upper side as depicted in Fig. 2, the unknown quantities are:

- $h_{W,4}$, $h_{W,7}$, $h_{W,8}$ ...incoming distribution functions in the water region,
- $h_{P,2}$, $h_{P,5}$, $h_{P,6}$ ...incoming distribution functions in the polymer region,
- ϕ_s ...value of the potential at the dielectric boundary.

In general, the distribution function h_α can be approximated as[21]

$$h_\alpha \cong h_\alpha^{\text{eq}} \lfloor 1 - \omega_\phi^{-1}(\boldsymbol{c}_\alpha \cdot \nabla) \ln h_\alpha^{\text{eq}} \rfloor. \quad (15)$$

Using the above equation, one can easily derive the following expressions that relate the potential and its derivative at the boundary.

$$\phi_s + \omega_\phi^{-1} \boldsymbol{c}_4 \cdot \nabla \phi_W|_s = 6(h_{W,2} + h_{W,5} + h_{W,6})$$
$$\phi_s + \omega_\phi^{-1} \boldsymbol{c}_2 \cdot \nabla \phi_P|_s = 6(h_{P,4} + h_{P,7} + h_{P,8}) \quad (16)$$

The right-hand-side terms of the above equations are known. Using eqns (13) and (16), one obtains an equation for ϕ_s:

$$(\varepsilon_W + \varepsilon_P)\phi_s = 6\varepsilon_W(h_{W,2} + h_{W,5} + h_{W,6}) + 6\varepsilon_P(h_{P,4} + h_{P,7} + h_{P,8}). \quad (17)$$

Once we know the potential ϕ_s at the boundary, $\{h_{P,\alpha}^{\text{eq}}\}$ and $\{h_{W,\alpha}^{\text{eq}}\}$ can be obtained from eqn (12) and the distribution functions can be obtained using the relation

$$h_\alpha + h_\beta = h_\alpha^{\text{eq}} + h_\beta^{\text{eq}} \; (\boldsymbol{c}_\alpha = -\boldsymbol{c}_\beta), \quad (18)$$

which is derived from eqn (15).

Boundary condition for the proton density

For the proton density distribution, a mid-grid bounce-back condition[36] was applied to maintain the zero-flux at the W–HS interface. Because of the nature of the mid-grid bounce-back scheme, the interface is assumed to lie between the neighboring lattice points. The flux perpendicular to the interface needs to be zero. Such a condition can be satisfied by using either stick or slip conditions at the boundary. However, the choice of stick or slip conditions is relevant to the flux parallel to the interface. Both the fluxes parallel and those perpendicular to the interface are always zero in the stick condition. In the slip condition, on the other hand, the flux parallel to the interface is not modified. The latter is physically more reasonable in diffusion problems. In general, the error caused by using the stick condition might be negligible. In the present case, however, it is expected that the stick condition causes significant reduction of the total flux because a large portion of the proton exists close to the boundary due to the attractive electrostatic force from the SO_3^- groups. The slip condition may be appropriate, as explained below.

The mid-grid bounce-back procedure can be regarded as a collision at the sub-lattice points between lattice points belonging to fluid (W) and solid (HS) regions at time $t = n + 1/2$ between successive time steps $t = n$ and $t = n + 1$, followed by a half-way streaming from sub-lattice points to the fluid region. Two types of sub-lattice points exist in the 2D9V lattice, as illustrated in Fig. 3, the points that intersect one fluid–solid link (open square) and the points shared by two fluid–solid links (full square). The latter type involves two unknown distribution functions (*e.g.*, in the situation shown in Fig. 3, distribution functions along 5 and 6 directions are unknown for full square points) with one "physical" condition, *i.e.*, the flux perpendicular to the interface is zero. Thus, one needs an artificial condition in order to complete the scheme. As discussed by He and Li,[21] the distribution functions at the lattice points satisfy the following relationship:

$$g_\alpha + g_{\alpha*} = g_\alpha^{\text{eq}} + g_{\alpha*}^{\text{eq}}. \quad (19)$$

In our case, the equilibrium distribution functions g_α^{eq} can be written as

$$g_\alpha^{\text{eq}} = W_\alpha \rho \left[1 - \left(\omega^{-1} - \frac{1}{2}\right) z \boldsymbol{c}_\alpha \cdot \nabla \phi\right]. \quad (20)$$

Inspection of the above expression reveals that the right-hand side of eqn (19) is independent of the velocity component, α. In fact, using $W_5 = W_6 = W_7 = W_8 = 1/36$, eqn (19) can be written as

$$g_7 + g_5 = g_8 + g_6 = \frac{1}{9}\rho. \quad (21)$$

If we assume that the distribution functions at the sub-lattice boundary points satisfy a similar relationship, *i.e.*,

$$g_7 + g_5 = g_8 + g_6 = K, \tag{22}$$

where K is an unknown constant that is independent of α, eqn (22) can be solved by combining with the zero-flux condition $g_5 + g_6 = g_7 + g_8$. The result is $g_5 = g_8$ and $g_6 = g_7$, which is identical to the slip condition. Therefore, we adopted the slip condition in all calculations in this paper. A comparison between the slip and stick conditions will also be given.

3. Results and discussion

3.1 Electrostatic potential with dielectric interfaces

To confirm that the boundary condition described in the previous section gives the correct behavior of the electrostatic potential at the dielectric interface, we calculated the electrostatic potential in a simple system, in which the image charge method can be used; a 2-D channel for a medium of dielectric constant ε_1 sandwiched by two media of dielectric constant ε_2, as shown Fig. 4a. A point charge Q_0 was placed at the center of the system. If the system length, L, is infinitely large, the effect of the dielectric interface is equivalent to placing an infinite series of image charges $Q_n = Q_{n-1}(\varepsilon_1 - \varepsilon_2)/(\varepsilon_1 + \varepsilon_2)$ $(n = 1, 2,\ldots,\infty)$ at positions $y_{\pm n} = y_0 \pm nR$ where y_0 and R are the positions of the real charge and the separation between two dielectric interfaces, respectively. We computed the electrostatic potential in the following situations:

- case A: The first set of image charges ($n = 1$) is placed.
- case B: Image charges up to $n = 5$ are placed.
- case C: Image charges up to $n = 10$ are placed.
- case D: The boundary condition given in section 2.4 is used instead of placing image charges.

Fig. 4 compares the calculated profiles of the electrostatic potential along the y-axis in cases A, B, C, and D. One can observe a good agreement between case B and case C, indicating that convergence of the image charge series is achieved. Because the result using our method (case D) agrees well with case C, we conclude that our treatment of the dielectric boundary works correctly.

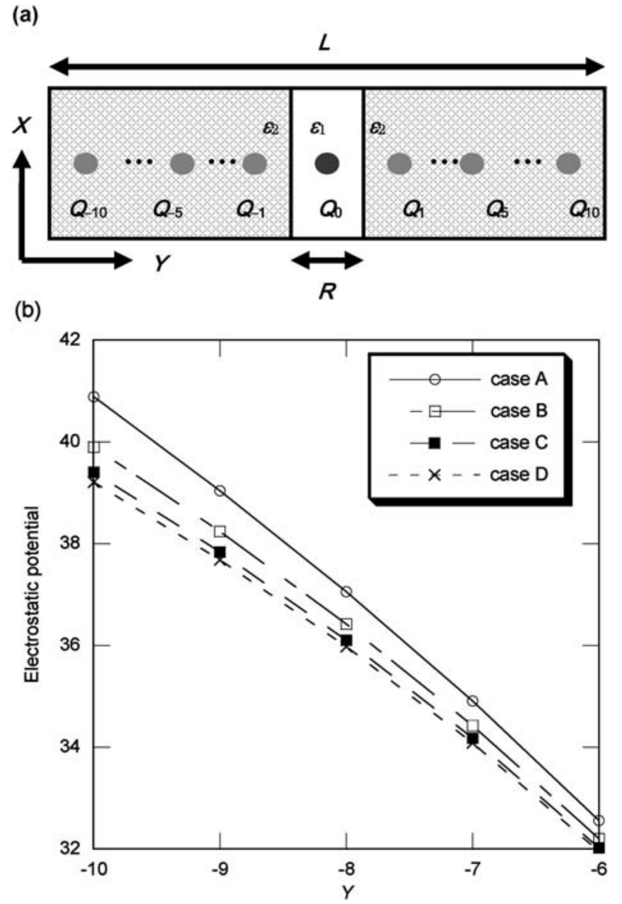

Fig. 4 Electrostatic potentials created by a point charge in a 2-D system with dielectric interfaces. (a) An illustration of the system. (b) The electrostatic potential profile calculated for the following situations: image charges $Q_{\pm 1}$ (see text for details) were placed (case A), image charges $Q_{\pm 1}$ to $Q_{\pm 5}$ were placed (case B), image charges $Q_{\pm 1}$ to $Q_{\pm 10}$ were placed (case C), and no image charges were placed and the discontinuity of the dielectric constant was taken into account by the method described in the text (case D). Q_0 is placed at $Y = 0$ and a dielectric interface lies at $Y = -10$. The following values were used: $R = 20$ lattice points, $L = 1000$ lattice points, $\varepsilon_1 = 78.0$, and $\varepsilon_2 = 7.09$.

3.2 Transport property of a proton in the model channel

3.2.1 The average mobility of a proton. The average proton mobility μ_{ave} through the channel was calculated for two structural parameters, the channel width R and the separation d of the SO_3^- groups. It was evaluated using the following expression:

$$\mu_{\text{ave}} = \frac{\langle j_x(\boldsymbol{r})\rangle_{\text{channel}}}{\langle \rho(\boldsymbol{r})\rangle_{\text{channel}} zeE_x}, \tag{23}$$

where E_x is the uniform electric field imposed along the x-axis to invoke the proton flow. The local flux $\boldsymbol{j}(\boldsymbol{r})$ was calculated as an average of the first-order moments of the pre-collision and post-collision distribution functions as

$$\boldsymbol{j}(\boldsymbol{r}_i) = \frac{1}{2}\sum_{\alpha}[g_{\alpha}^{\text{pre-collision}}(\boldsymbol{r}_i) + g_{\alpha}^{\text{post-collision}}(\boldsymbol{r}_i)]\boldsymbol{c}_{\alpha}, \tag{24}$$

because momentum is not collision-independent in the diffusion LBM. The value of $|\boldsymbol{E}|$ was taken to be small enough so that μ_{ave} is independent of $|\boldsymbol{E}|$. $|\boldsymbol{E}| = (kT/e) \times 10^{-3}$ per Å was adopted for all calculations. An approximate expression for μ_{ave} up to a first order in $|\boldsymbol{E}|$ is derived in the Appendix using a perturbation expansion.

SO_3^- groups in the present model are represented by line charges instead of point charges because a 2-D model was used. Because the electrostatic potential created by a line charge is much more long-ranged than is the case of a point charge, a periodic array of line charges creates a smoother (in other words, more homogeneous) electrostatic potential profile compared to a periodic array of point charges. This means that the potential gradient $\nabla\phi_0$ in the 2-D system becomes smaller than in 3-D space. Therefore, according to eqn (A3), it is expected that the resistance to proton motion due to the SO_3^- charges is underestimated in the present 2-D system.

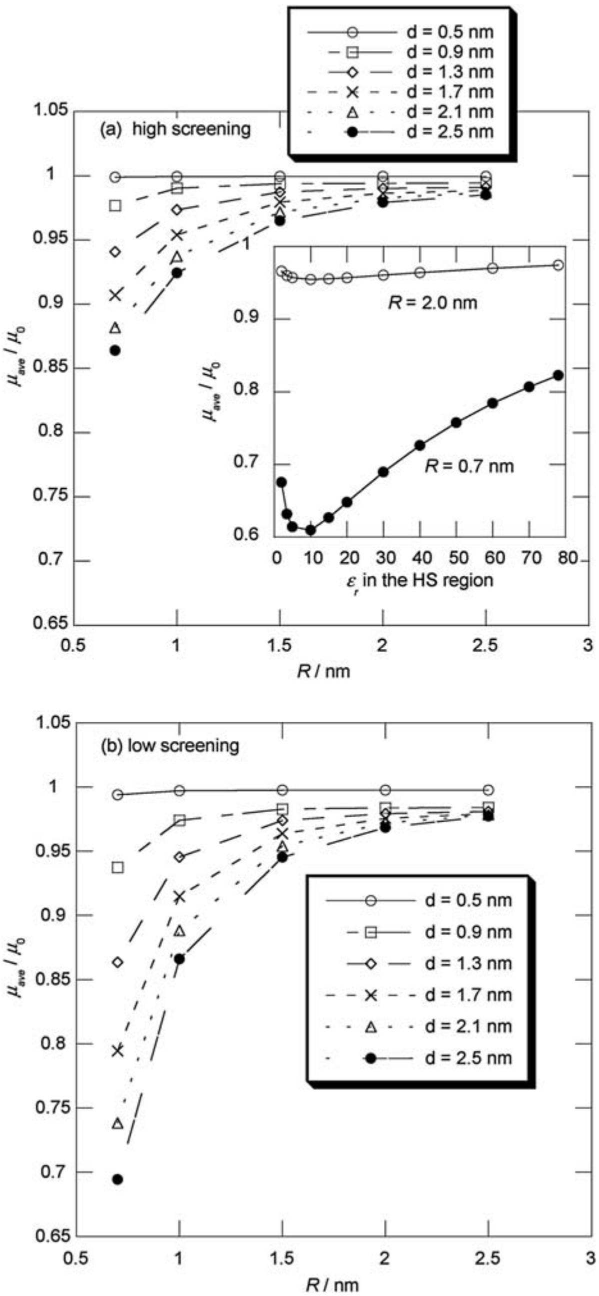

Fig. 5 Ratio of the average mobility $\mu_{\rm ave}$ to the bulk mobility μ_0 as a function of the channel width R for various values of the separation d of the SO_3^- groups. (a): high screening of SO_3^- charges by hydration shells (ε_r = 78.0 in the HS region), (b): low screening of SO_3^- charges by hydration shells (ε_r = 2.0 in the HS region). ε_r of the water region where the proton can move was set to 78.0 for both cases. The slip boundary condition was used. $\mu_{\rm ave}/\mu_0$ as a function of the dielectric constant of the HS region is plotted in the inset of Fig. 5a.

3.2.2. Dependency on the channel width and the separation of the SO_3^- groups. First, we show the results obtained using the slip boundary condition. Fig. 5 plots the ratio of $\mu_{\rm ave}$ to the bulk mobility μ_0 as a function of the channel width R for several values of the separation d of the SO_3^- groups. Fig. 5a and b correspond to two different values of ε_r in the HS region having high and low screenings effects. It is seen that $\mu_{\rm ave}$ approaches μ_0 as R increases and d decreases. As the water content increases, *i.e.* R increases, the channels in the membrane are filled by a large number of water molecules and therefore the environment for the proton in the channels becomes like that of bulk water. The dependency of $\mu_{\rm ave}$ on R shown in Fig. 5 agrees with such a general relationship between the proton conductivity and water content of the membrane.

In Fig. 6, the electrostatic potential profiles that the proton experiences along the direction of the proton path are plotted for R = 7 Å and various values of d. The potentials plotted in Fig. 6 are measured on the lattice plane next to the W–HS interface. It is seen that the proton feels a higher potential barrier in the channel with large d. By comparing this with the dependency of $\mu_{\rm ave}$ on d which is shown in Fig. 5, one can observe a clear correspondence between $\mu_{\rm ave}/\mu_0$ and the barrier height of the electrostatic potential that the proton needs to overcome; that is, $\mu_{\rm ave}$ is reduced for a larger potential barrier. From Fig. 6 it is obvious that with a large barrier, the potential has a large gradient. Therefore, deviation of $\mu_{\rm ave}$ from μ_0 is determined by the magnitude of $\nabla\phi_0$, as shown in the Appendix.

Fig. 5 also reveals that $\mu_{\rm ave}$ depends on R more strongly when d becomes larger, because of the higher electrostatic potential barrier with larger values of d. This agrees with the calculations carried out by Eikerling *et al.* using a 3-D channel with a slab-like structure.[13] One can also observe that as R decreases $\mu_{\rm ave}/\mu_0$ deviates from 1.0 more rapidly for larger d. For example, $\mu_{\rm ave}/\mu_0$ is almost constant for d = 5 Å. In the case of d = 25 Å, on the other hand, $\mu_{\rm ave}/\mu_0$ varies considerably over a wide range of R. This can be understood in terms of the magnitude of R relative to d; if d is considerably smaller than R, which is the characteristic length of the channel, the electrostatic potential created by SO_3^- charges becomes flat along the x-direction. On the other hand, when d is larger than the characteristic length, the proton in the channel recognizes the discreteness of the SO_3^- charges, and therefore, feels higher potential barriers.

Fig. 5b indicates that the low screening condition (ε_r = 2 in the HS region) leads to a significant reduction of $\mu_{\rm ave}/\mu_0$, indicating that the proton experiences a higher barrier for the electrostatic potential because of the SO_3^- group in the low screening case. Intuitively, the lower the screening of the SO_3^- charge, the higher the potential barrier that the proton can feel. Because the SO_3^- charge is placed between the W–HS interface and the HS–P interface, one has two series of image charges of SO_3^- groups created in the W and P regions. The image charges in both regions raise the magnitude of the electrostatic field at the W–HS interface, and hence, reduce $\mu_{\rm ave}/\mu_0$.[37] The image charges in the W region are stronger for lower ε_r of HS. The image charges in the P region, on the other hand, are weaker for low ε_r of HS. Thus, there are two competing effects because of the W–HS and HS–P interfaces. In the inset of Fig. 5a, $\mu_{\rm ave}/\mu_0$ is plotted as a function of ε_r of HS for R = 7 and 20 Å at d = 21 Å. It is seen that the behavior of $\mu_{\rm ave}/\mu_0$ for ε_r, which is larger than ~10.0, is mostly affected by the W–HS interface. For small values of ε_r, the effect of the HS–P interface turns out to be more significant.[38]

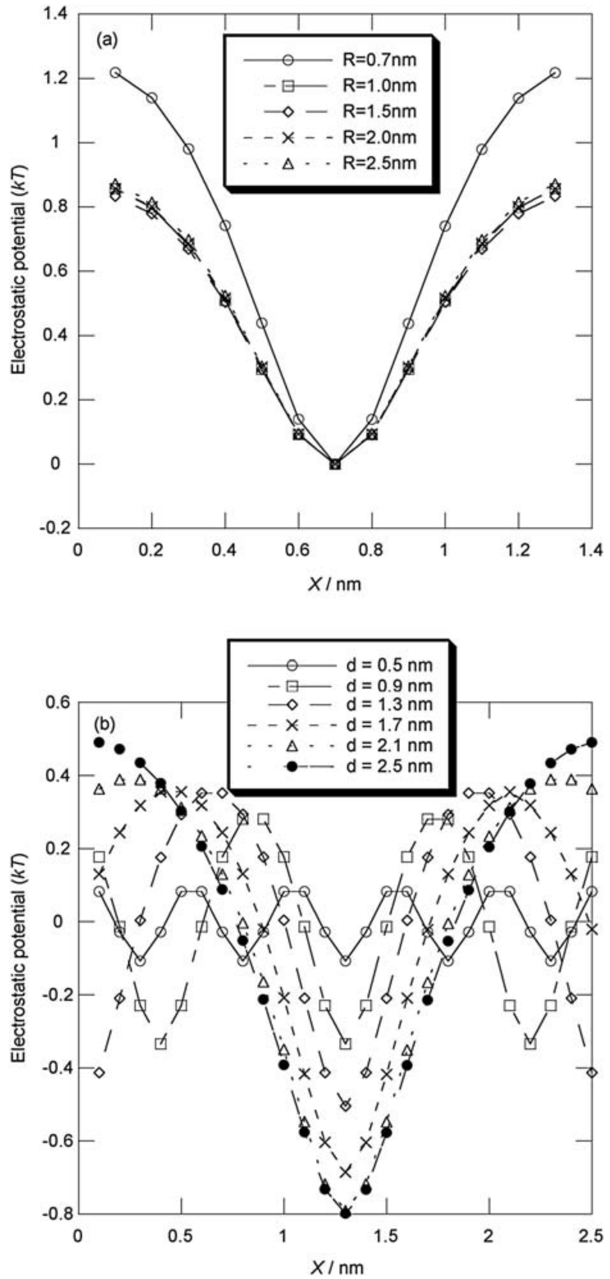

Fig. 6 Variation of the electrostatic potential ϕ in the channel along the direction of the external electric field $\boldsymbol{E}$. Each profile of ϕ was measured on the plane next to the W–HS interface. (a) Profiles of ϕ with various values of R for d = 9 Å and (b) profiles of ϕ with various values of d for L = 24 Å and R = 20 Å.

In Fig. 7, the proton density change $\delta\rho$ induced by the uniform electric field $\boldsymbol{E}$ is plotted together with the electrostatic potential resulting from the charge distribution (SO_3^- charge plus proton distribution). The arrow indicates the direction of $\boldsymbol{E}$. From Fig. 7, one can obtain a clear insight into the physical origin of the reduction of μ_{ave} from μ_0. The average position of the proton is shifted along the direction of $\boldsymbol{E}$. The electrostatic potential resulting from the SO_3^- charge, on the other hand, tends to restore the proton to the original position. Such a restoring force by the SO_3^- charges is the origin of the reduction of μ_{ave} from μ_0.

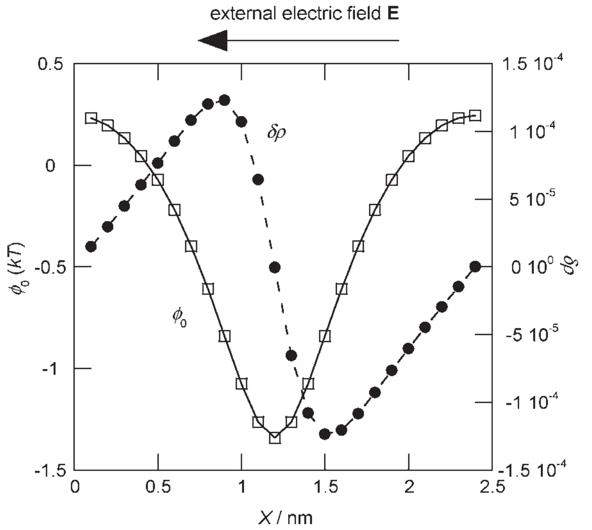

Fig. 7 Density change $\delta\rho$ (full circles) induced by applying a uniform external electric field E_x in the direction parallel to the channel wall and the electrostatic potential ϕ_0 (open squares) created by the charge density (SO_3^- charges plus proton density distribution). The values on the lattice plane next to the W–HS interface are plotted. The arrow indicates the direction of E_x. The structure of the channel is R = 20 Å and d = 24 Å.

μ_{ave}/μ_0 computed using the stick boundary condition is plotted in Fig. 8. Because the stick condition forces the flux parallel to the boundary to be zero at the boundary, there is no contribution to the total flux from the protons located at the boundary. Therefore, the values of μ_{ave}/μ_0 plotted in Fig. 8 are lower than the values in Fig. 5, especially when the channel width R is small. It is expected that, as the ratio of the area of boundary to the volume of fluid domain increases (that is, for smaller R), the influence of using the stick condition will become more significant. Moreover, for the case of proton diffusion in Nafion, a large portion of the proton is located near the W–HS boundary because of the electrostatic attractive force resulting from the SO_3^- charges. We also note that the proton located at the boundary feels the highest electrostatic potential barrier within the channel. As we discussed earlier, deviation of μ_{ave} from μ_0 is strongly related to the electrostatic potential barrier. Therefore, an appropriate treatment of the local flux at the boundary is critical to estimating the proton conduction of the whole system. Fig. 8 implies that μ_{ave}/μ_0 calculated with the stick condition is much less sensitive to the channel structure, because the flux at the boundary, the most important contribution to the total flux that determines the behavior of μ_{ave}/μ_0 as a function of channel structure, is ignored by using the stick condition. Therefore we conclude that the stick condition should be avoided or used with extreme caution (recognizing that the result is more insensitive to the structure) in simulating the proton conduction in Nafion with low water content.

Molecular dynamics (MD) simulations have been applied to Nafion by several authors.[39–42] Dupuis and coworkers demonstrated that the diffusion coefficient of H_3O^+ ion in a low water-content membrane (λ = 3.5 and 6) is reduced from that in a high water-content membrane (λ = 16) by a factor of

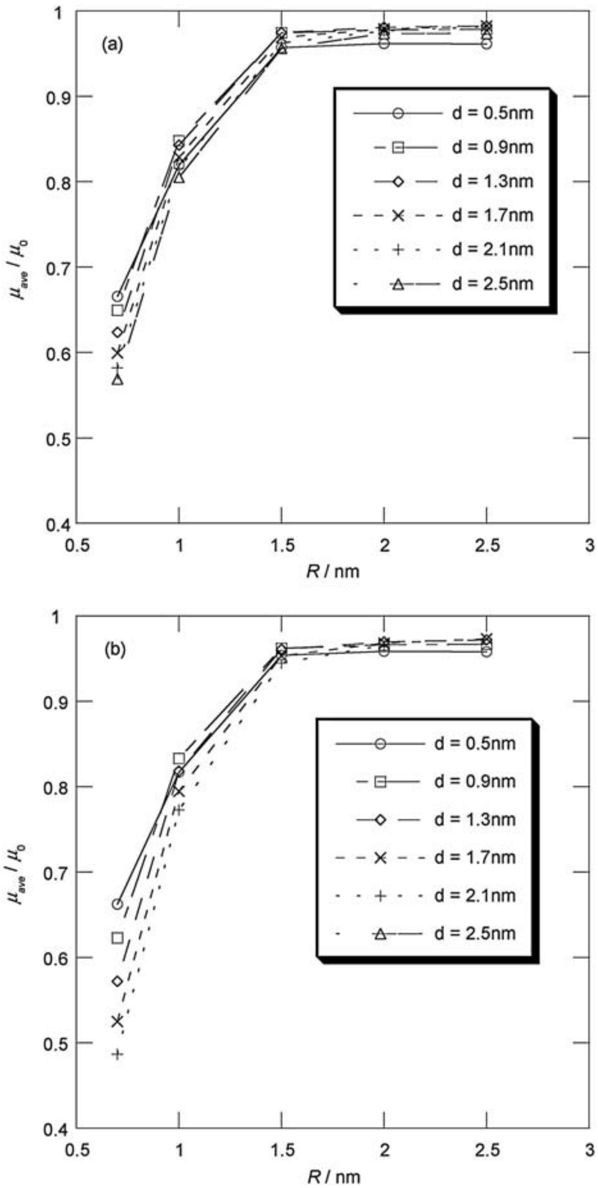

Fig. 8 The average mobility μ_{ave} obtained with the stick boundary conditions. Other conditions are the same as those in Fig. 5.

two to three, though they used a classical force field and, as a result, the Grotthuss mechanism was not taken into account.[40] Hofmann and coworkers used a reactive force field so that the Grotthuss proton hopping was taken into account.[41] They obtained 3.2×10^{-6} cm^2 s^{-1} and 10.5×10^{-6} cm^2 s^{-1} as the value of the diffusion coefficient of proton in the Nafion membrane with $\lambda = 6$ and 12, respectively. These MD studies illustrate that the conductivity of the low-water-content membrane is 30 to 50% of that of the high-water-content membrane. Our results shown in Fig. 5b also indicate that proton diffusivity of the low water-content membrane (R = 7 Å) is $\sim$70% of the bulk value. We note that dependencies of μ_{ave}/μ_0 on R shown in Fig. 5 and 8 are very weak compared to the values obtained by MD simulations. In the present calculation a uniform relaxation time τ for the BGK collision was used, based on the assumption that the mobility ($\sim 1/\tau$) of the proton has the same value everywhere. Under such an assumption, the direct electrostatic attractive interaction between the proton and SO_3^- charges is the only factor that reduces the overall conductance of the channel. The random porous structure involved in MD simulations also inhibits proton conduction; however, such an effect is not involved in straight channel models.

Hindrance of the proton motion by the restoring force resulting from the SO_3^- charges can be attributed to the direct interaction to SO_3^- groups in the model of Paddison and coworkers.[8] According to their calculations,[11] the average mobility of the proton increases monotonically as the SO_3^- groups are distributed more homogeneously in a 3-D cylindrical channel. Our results shown in Fig. 5 qualitatively agree with those by Paddison and coworkers, in spite of the simplified 2-D model in the present work.

As described in section 2.1, the relative dielectric constant ε_r in the W region was assumed to have the value of bulk water irrespective of the value of the channel width R. The effect of the dielectric saturation was reflected to small values (2 in the low-screening case) of ε_r in the HS region. Our choice of ε_r values is based on the works by Paul and Paddison, in which the profile of ε_r as a function of radial distance from the center of a cylindrical channel was estimated.[25–27] Their results indicate that while ε_r is quite small (less than 10) in the proximity of SO_3^- group due to strong dielectric saturation, it is close to the value of bulk water around the channel center even when the water content is small (λ = 6). The fact that ε_r in the channel center is close to the value of bulk water even for the low water content is rather unexpected, because the environment of the water molecules in such a small channel should be significantly different from that in large channels. One could expect that ε_r in the channel center deviates much more from the value of bulk water in the case of a channel with low water content. This might partly explain the smaller dependencies obtained for μ_{ave}/μ_0 on R than the experimental ones. It should be noted, however, that the above discussion about the possibility of reducing the value of ε_r in the W region for low water content channels is a purely intuitive one. The value of the physical parameter should be selected based on the available literature.

Another important factor to be considered is the local mobility of the proton. In the present calculation, the uniform relaxation time τ in the BGK collision term was employed; that is, τ does not depend on position. Because τ is equivalent to the diffusion coefficient (and therefore, equivalent to the mobility), this means that we assumed *a priori* that the mobility of the proton takes the same value everywhere in the channel. We know *a posteriori* that the average mobility μ_{ave} changes from the initially assumed μ_0. However, it is expected that the mobility of the proton is strongly affected by the local environment such as solvent water molecules around the proton and the distance from the nearest SO_3^- group. As demonstrated by Eikerling *et al.*,[13,14] it is critically important for a quantitative estimation of membrane conductance that one has information on the nonuniform local mobility *a priori.* Such information may be derived, for example, by a first principles simulation. Once we have knowledge of the local mobility in the whole system, it is trivial to incorporate such information into the LBM calculation. We note that the LBM has been shown to work well with a nonuniform relaxation time.[16]

As stated in section 2, the LBM can handle any structures with no additional computational demands. Therefore, it is possible to extend the present work to analyse the disordered porous structure of Nafion which can be obtained by dissipative particle dynamics simulations.[43] Using such a 3-D "real structure" of the membrane, it is possible to evaluate the membrane conductance directly by the present method. This capability of the LBM will enable the present scheme to evaluate the performance of PEFC systems.

4. Conclusions

In this paper we have developed a 2-D LBM scheme for electromigration–diffusion systems for the purpose of developing a simulation method for proton conduction in PEMs. The average mobility μ_{ave} of the proton in a nonequilibrium stationary state in which a uniform external electric field was applied to induce a current was evaluated using the 2-D channel of a slab-like structure. The behavior of μ_{ave} as a function of the channel width R and the separation d of the SO_3^- groups was analyzed. Large dependencies of μ_{ave} on those structure parameters were observed, especially when d was changed. Our results illustrate that while the proton density distribution at the equilibrium state is shifted by the uniform external field, the attractive force resulting from SO_3^- groups tends to restore the shifted density distribution to the original distribution, and thus the average mobility of the proton is considerably reduced from the mobility in bulk water. The dependencies of μ_{ave} on R and d agree qualitatively with the perturbation analysis. Although we used the slip condition, which is appropriate for diffusion problems, the validity of the conventional stick boundary condition was also examined. It was shown that the results obtained using the stick condition are much less sensitive to channel structure. Using the stick condition should be avoided for narrow channels.

It is possible to adapt the present scheme to real membrane structures. It is expected that our LBM scheme for electromigration–diffusion systems will provide a powerful tool for simulating the proton transport phenomenon in PEFC systems. Calculations with more realistic models involving extension to 3-D systems are now in progress.

Appendix

In this Appendix we see the physical meaning of our calculations by means of a perturbation expansion. If we assume that the external electric field is much smaller than the electrostatic field resulting from the charge density (SO_3^- charges plus proton density), *i.e.*, $|\boldsymbol{E}| = \lambda|\nabla\phi_0| \approx \lambda E_0$ where $\lambda \ll 1$ and E_0 is the characteristic magnitude of $\nabla\phi_0$, the proton density distribution $\rho(\boldsymbol{r})$ in the presence of $\boldsymbol{E}$ can be expanded as follows:

$$\begin{aligned}\rho(\boldsymbol{r}) &= \rho_0(\boldsymbol{r}) + \delta\rho(\boldsymbol{r}) \\ &\equiv \rho_0(\boldsymbol{r}) + \lambda\rho_1(\boldsymbol{r}) + \lambda^2\rho_2(\boldsymbol{r}) + \cdots, \end{aligned} \quad \text{(A1)}$$

where ρ_0 is the proton density distribution at the equilibrium state. The flux of the proton in the presence of $\boldsymbol{E}$ can be written as a follows up to the first order of λ:

$$j_x(\boldsymbol{r}) = -D_0\Big[\lambda\Big\{\nabla\rho_1 + \frac{ze}{kT}(\rho_1\nabla\phi_0 + \rho_0 E_0)\Big\} + O(\lambda^2)\Big], \quad \text{(A2)}$$

where D_0 is the proton diffusion coefficient in bulk water. By introducing eqn (A2) into eqn (23), we obtain the following expression for μ_{ave} in the limit $\lambda \to 0$:

$$\mu_{\text{ave}} = \frac{\mu_0}{NE_0}\int(\nabla\phi_0)\rho_1 \mathrm{d}\boldsymbol{r} + \mu_0, \quad \text{(A3)}$$

where $\mu_0 \equiv D_0/kT$ is the proton mobility in bulk water, and N is the total number of protons in the unit cell. The second term on the right-hand side of eqn (A3) represents the zeroth-order approximation for μ_{ave}; that is, ignoring the first-order density derivative ρ_1, one obtains the bulk mobility μ_0 as the average mobility. Actually, μ_{ave} deviates from μ_0 because of the nonzero density change $\delta\rho$ induced by the applied field $\boldsymbol{E}$, according to the first term on the right-hand side of eqn (A3). We note that eqn (A3) was obtained at the nonequilibrium stationary state with a nonzero flow.

References

1 K. A. Mauritz and R. B. Moore, *Chem. Rev.*, 2004, **104**, 4535, and references therein.
2 B. C. H. Steele and A. Heinzel, *Nature*, 2001, **414**, 345.
3 K.-D. Kreuer, S. J. Paddison, E. Spohr and M. Schuster, *Chem. Rev.*, 2004, **104**, 4637.
4 R. Jinnouchi and K. Okazaki, *J. Electrochem. Soc.*, 2003, **150**, E66.
5 S. Urata, J. Irisawa, A. Takada, W. Shinoda, S. Tsuzuki and M. Mikami, *J. Phys. Chem. B*, 2005, **109**, 17274.
6 Y.-K. Choe, E. Tsuchida, T. Ikeshoji, S. Yamakawa and S. Hyodo, submitted.
7 X.-D. Din and E. E. Michaelides, *AIChE J.*, 1998, **44**, 35.
8 S. J. Paddison, R. Paul and T. A. Zawodzinski, Jr, *J. Electrochem. Soc.*, 2006, **147**, 617.
9 S. J. Paddison, R. Paul and K.-D. Kreuer, *Phys. Chem. Chem. Phys.*, 2002, **4**, 1151.
10 S. J. Paddison and R. Paul, *Phys. Chem. Chem. Phys.*, 2002, **4**, 1158.
11 S. J. Paddison, R. Paul and T. A. Zawodzinski, Jr, *J. Chem. Phys.*, 2001, **115**, 7753.
12 R. Paul and S. J. Paddison, *J. Chem. Phys.*, 2005, **123**, 224704.
13 M. Eikerling and A. A. Kornyshev, *J. Electroanal. Chem.*, 2001, **502**, 1.
14 M. Eikerling, A. A. Kornyshev, A. M. Kuznetsov, J. Ulstrup and S. Wallbran, *J. Phys. Chem. B*, 2001, **105**, 3646.
15 P. Choi, N. H. Jalani and R. Datta, *J. Electrochem. Soc.*, 2005, **152**, E123.
16 D. A. Wolf-Gladrow, in *Lattice–Gas Cellular Automata and Lattice Boltzmann Models*, Springer-Verlag, Berlin Heidelberg, 2000.
17 S. Succi, in *The Lattice Boltzmann Equation for Fluid Dynamics and Beyond*, Oxford University Press, Oxford, 2001.
18 R. G. M. van der Sman and M. H. Ernst, *J. Statist. Phys.*, 1999, **94**(1/2), 203.
19 B. Li and D. Y. Kwok, *Int. J. Heat Mass Transfer*, 2003, **46**, 4235.
20 S. Melchionna and S. Succi, *J. Chem. Phys.*, 2004, **120**, 4492.
21 X. He and N. Li, *Comput. Phys. Commun.*, 2000, **129**, 158.
22 S. J. Paddison, D. W. Reagor and T. A. Zawodzinski, Jr, *J. Electroanal. Chem.*, 1998, **459**, 91–97.
23 S. J. Paddison, G. Bender, K.-D. Kreuer, N. Nicoloso and T. A. Zawodzinski, Jr, *J. New Mater. Electrochem. Syst.*, 2000, **3**, 293–302.
24 Z. Lu, G. Polizos, D. D. Macdonald and E. Manias, *J. Phys. Chem. B*, 2008, **155**, B163–B171.
25 R. Paul and S. J. Paddison, *J. Chem. Phys.*, 2001, **115**, 7762.
26 R. Paul and S. J. Paddison, *Solid State Ionics*, 2004, **168**, 245–248.

27 R. Paul and S. J. Paddison, *J. Phys. Chem. B*, 2004, **108**, 13231–13241.
28 J. N. Israelachvili, in *Intermolecular and Surface Forces*, Academic Press, 2nd edn, 1992, ch. 5.
29 D. Eisenberg and W. Kauzmann, in *The Structure and Properties of Water*, Oxford at Clarendon Press, London, 1969, ch. 4.
30 Y.-K. Choe, E. Tsuchida, T. Ikeshoji, S. Yamakawa and S. Hyodo, personal communication.
31 W. H. Press, S. A. Teukolsky, W. T. Vetterling and B. P. Flannery, in *Numerical Recipes in Fortran*, Cambridge University Press, Cambridge, 1994, pp. 857–880, ch. 19.
32 J. L. Thomas, B. Diskin and A. Brandt, *Annu. Rev. Fluid Mech.*, 2003, **35**, 317.
33 H.-G. Haubold, Th. Vad, H. Jungbluth and P. Hiller, *Electrochim. Acta*, 2001, **46**, 1559.
34 B. Dreyfus, G. Gebel, P. Aldebert, M. Pineri, M. Escoubes and M. Thomas, *J. Phys. (Paris)*, 1990, **51**, 1341.
35 J. D. Jackson, in *Classical Electrodynamics*, John Wiley & Sons, 1975, ch. 4.
36 A. J. C. Ladd, *J. Fluid Mech.*, 1994, **271**, 285.
37 Image charges in the W region strengthen the electrostatic field at the W–HS interface because they have the opposite sign to the real charge, which is in the HS region. Image charges in the P region have the same sign as the real charge, therefore they weaken the electrostatic field at the HS–P interface; however, the electrostatic field at the W–HS interface is strengthened.
38 We estimated the magnitude of the electrostatic field at the W–HS interface as a function of ε_r of HS for a 3-D case, by ignoring the proton distribution and using the image charge technique. The result indicates that although there is still a minimum of μ_{ave}/μ_0 at small ε_r of HS, it is less pronounced than for the 2-D case. Therefore, the effect of varying ε_r of HS can be expected to be well explained by considering only the W–HS interface in a 3-D system.
39 E. Spohr, P. Commer and A. A. Kornyshev, *J. Phys. Chem. B*, 2002, **106**, 10560–10569.
40 A. Venkatnathan, R. Devanathan and M. Dupuis, *J. Phys. Chem. B*, 2007, **111**, 7234–7244.
41 D. W. Hofmann, L. Kuleshova and B. D'Aguanno, *J. Mol. Model.*, 2008, **14**, 225–235.
42 M. K. Petersen and G. A. Voth, *J. Phys. Chem. B*, 2006, **110**, 18594–18600.
43 S. Yamamoto and S. Hyodo, *Polym. J.*, 2003, **35**, 519.

